JOURNAL OF CATALYSIS 115, 473–485 (1989)

Microstructure of Pt–Rh Particles on SiO_2[1]

T. P. CHOJNACKI AND L. D. SCHMIDT

Department of Chemical Engineering and Material Science, University of Minnesota, Minneapolis, Minnesota 55455

Received May 10, 1988; revised August 2, 1988

The microstructure of 20- to 200-Å Pt–Rh alloy particles on amorphous SiO_2 have been examined by transmission electron microscopy and electron diffraction following heat treatments in H_2, O_2, He, and N_2 atmospheres. It was observed that, upon formation of particles in H_2 at temperatures between 600 and 100°C, a two-phase structure exists within essentially all particles. One phase is a section of a cube, exactly as noted previously for pure Pt particles. The other phase is a highly twinned region usually with a single set of multiple twin bands <10° Å wide. When these phase-separated samples were heated in N_2 or He, single-phase particles with shapes between polyhedra and spheres were observed. Subsequent heating in H_2 restores the two-phased morphology. Mild heating at 300°C in O_2 results in the breakup of the twinned regions but causes no significant change to the cube-shaped regions. Particles grown from metal films or from the salts of $RhCl_3$ and H_2PtCl_6 or $[Pt_3(CO)_6]_4^{2-}$ are found to have essentially identical microstructures upon heating to 600°C.

INTRODUCTION

Supported alloy catalysts have frequently been found to possess properties superior to those of the individual metals. As examples, Pt–Ir and Pt–Re have higher selectivity and a greater coke resistance in hydrocarbon reforming than Pt alone (*1–4*), and Pt–Rh is better in NH_3 oxidation in the production of HNO_3 (*5*) and in the removal of NO in automotive catalysts (*6*) than either metal. A knowledge of the correlation between differences in composition and microstructure is therefore crucial in understanding their catalytic properties.

We have previously shown, using transmission electron microscopy (TEM), that the morphology of supported metal catalysts can be dramatically altered by different gas treatments (*7, 8*). This work has shown the exclusive formation of 20- to 200-Å Pt cubes (*7*) with (100) faces and (100) planes in contact with SiO_2 and γ-Al_2O_3 if grown in H_2 at 650°C. In contrast, treatment in nitrogen or oxygen at this temperature produces polyhedral or spherical particles. Hydrogen or nitrogen treatment of Rh on silica produces hexagonally shaped particles, while heating in O_2 forms Rh_2O_3, and low-temperature H_2 treatment produces clusters of small Rh particles (*8*).

In earlier work on Pt–Rh alloys (*9*) we examined by TEM the effects of H_2 and O_2 treatments on the morphology of small alloy particles. We observed particles with an irregular polyhedral shape and many twins as a result of heat treatment in nitrogen. We also showed that treatment of those alloy particles in air above 400°C resulted in the formation of a Rh_2O_3 layer on the surface of the particles and that subsequent low-temperature reduction produced a Rh-enriched surface layer.

Recently we have shown that microstructure has a significant influence on the catalytic activity of support metals. Specifically, CO hydrogenation rates decrease as the number of high-index planes increases for Ni on SiO_2 (*10*), while ethane hydrogenolysis activity increases as particle irregularity increases for Rh and other metals on SiO_2 (*11*).

[1] This research was partially supported by the National Science Foundation under Grant CBT 8518652.

0021-9517/89 $3.00

Alloy surfaces and particles should in general be expected to exhibit a surface enrichment of one species such that the lower surface tension, lower melting metal (Pt for Pt–Rh alloys) should have a high concentration at the surface. Similar arguments hold for systems which are immiscible in the bulk, and it has been shown that sufficiently small particles appear to be miscible even when they exhibit low-bulk solubility (*12*).

We report here results of a study of the Pt–Rh system on SiO_2. This work was begun to determine the shapes of Pt–Rh alloy particles and in particular to determine whether alloy particles might be cube-shaped as was found for pure Pt particles (*7*). We observed a much more complicated situation of phase separation upon treatment in H_2 at elevated temperatures even though all published phase diagrams of Pt–Rh show only a single-phase alloy at all compositions (*13, 14*).

EXPERIMENTAL

The amorphous silica substrate was prepared by first covering gold TEM grids with a thin Formvar film upon which 140- to 200-Å-thick silicon films were vacuum deposited. The films were then oxidized in a quartz tube furnace under a flow of oxygen at 800°C for a ~36 hr to burn off the Formvar and produce an amorphous silica substrate <300 Å thick. Metals were deposited separately by vacuum deposition of Pt and Rh in such a manner that only platinum was deposited on one-half of a TEM sample grid as a control while both Pt and Rh were deposited on the other half to produce the alloy. The order of deposition of the metals was found to be insignificant in the breakup of the film and structures of the resultant particles if heated up to 1000°C. Metal film thicknesses of 10 to 30 Å were calculated by assuming uniform evaporation from a point source, and alloy compositions were regarded as accurate to within ±15%.

The alloy was also prepared from aqueous $RhCl_3$–PtH_2Cl_6 solutions. Pt and Rh were also prepared from solutions of $[Pt_3(CO)_6]_4^{2-}$ in dried, N_2-purged methanol and aqueous $RhCl_3$, respectively. Depositions from aqueous solution were carried out by first placing a TEM sample grid on nonwetting Parafilm with the silica side up. Then a drop of solution containing a calculated amount of salt was placed on the grid in such a manner so that the entire drop would bead up on the silica. Depositions from a nonaqueous solution were done in a similar manner with a glass slide replacing the Parafilm. Samples were then heated to evaporate solvents and decompose the salts.

Samples were heated in a quartz tube at temperatures ranging from 300 to 1000°C for varying times with gases at atmospheric pressure flowing through the furnace at a rate of ~50 cm^3/min. Ultrahigh-purity hydrogen (99.999%) and oxygen (99.995%) were used without further purification. Nitrogen (99.995%) was further purified by passing it through a H_2O/O_2 scavenging gas purifier, while helium (99.995%) was passed though a molecular sieve trap cooled to 80 K.

Samples were analyzed in a JEOL 100CX TEM equipped with a scanning attachment which enabled the use of a 150-Å beam size for microdiffraction. Samples could be treated in the furnace, observed by TEM, and retreated such that *the same particles* could be examined repeatedly in sequential treatments. Because amorphous silica produced intense diffuse rings in the electron diffraction patterns, the technique of unsharp masking (*15, 16*) was used to enhance diffraction rings of the metals.

RESULTS

Growth in Hydrogen

Heating of the Pt–Rh films for several hours in hydrogen at 650°C produced particles in which essentially all had segregated into two or more regions. These are of two types: a region of the particles exhibiting a section of a cube and a region being generally spherical and highly defected. This is

illustrated by the TEM micrograph of a 38 at.% Rh alloy sample in Fig. 1a. In all samples examined after this treatment more than 65% of the particles could be identified as exhibiting this segregated structure.

It is of course difficult to determine particle shapes from images alone. The particle outlines are clearly determined, but thicknesses are not related to contrast because of diffraction effects. In previous examinations of Pt particles on SiO_2, we used weak beam dark field fringes to show that the tops of the particles are flat and that the edges [(110) planes] are approximately 45° to the tops (7). In fact, thickness contrast fringes are evident in some of the bright field micrographs shown here. In the alloys the Pt regions appear slightly darker than the alloy region as expected from greater scattering from Pt than Rh, and we infer that particle heights are approximately the same for both regions. In the interpretation of these results we rely exclusively on particle outlines and the positions of the boundary between regions to infer the structure.

Dark field imaging of the same area (Fig. 1b) using the (200) diffraction ring of fcc (Pt and Rh) revealed that the defected regions are confined exclusively to the "spherical" parts of the particles and appear to be due to stacking faults while the cubic regions are single crystals with no defects. Microdiffraction patterns of the cubic regions show them to be fcc with a [100] zone axis, as seen in diffraction pattern of region 1 of Fig. 1b. Inset 2 shows a microdiffraction pattern of a typical defected region, which is sharp in one direction and streaked in the other, thus confirming the formation of stacking faults in these areas of the particles. The micrographs show that the (111) plane of the cubic structure is the preferred segregation boundary for the majority of these particles, while the stacking faults generally lie perpendicular to the [111] direction of the cubic structure.

The TEM micrographs of Fig. 2 show the evolution of particle structures following hydrogen treatment of a typical 44 at.% Rh sample at increasing temperatures. Segregated particles showing the characteristic cubic and defected regions are formed from the evaporated film after heating for 4 hr at 650°C in H_2 (Fig. 2a). Additional treatment at 800°C for 1 hr results only in the regions assuming a more regular shape (Fig. 2b). Further hydrogen treatment for 5 hr at 850°C produces no change except for the transformation of several particles exhibiting three regions into two-region particles as indicated by arrows in Fig. 2b and 2c. Here the three-region particles having two cubic regions separated by a defected region transform into two-region particles in which one cubic section grows while the other disappears. Note that one particle forms a twinned cubic region.

Further treatment for 22 hr at 850°C and 5 hr at 900°C produces less streaking in the bright field images as shown in Figs. 2d and 2e, which is accompanied by a decrease in the streaking of the diffraction rings assigned to the alloy, a change indicative of an increase in the ordering of the defected areas. Segregation persists up to 1000°C where treatment for 17 hr results in significant coalescing of the defected regions and the formation of particles which now appear to be twinned (Fig. 2f). Similar results were observed for all Pt–Rh alloys containing <50% Rh, although, as expected, the relative size of the cubic region for the particles in these samples was greater for higher Pt loadings.

Throughout a H_2 treatment sequence, electron diffraction always revealed the rings due to Pt metal; the assignment of these rings was confirmed each time by examination of the Pt half of the sample grid. As indicated in Fig. 3, an additional complex pattern of rings attributed to the alloy was also present. Initially the alloy rings appeared broadened or streaked, particularly the low-index reflections. As the temperature increased, the degree of streaking decreased along with the decrease in the disorder of the alloy regions as observed in the TEM image. However, two sets of fcc rings persisted up to 1000°C.

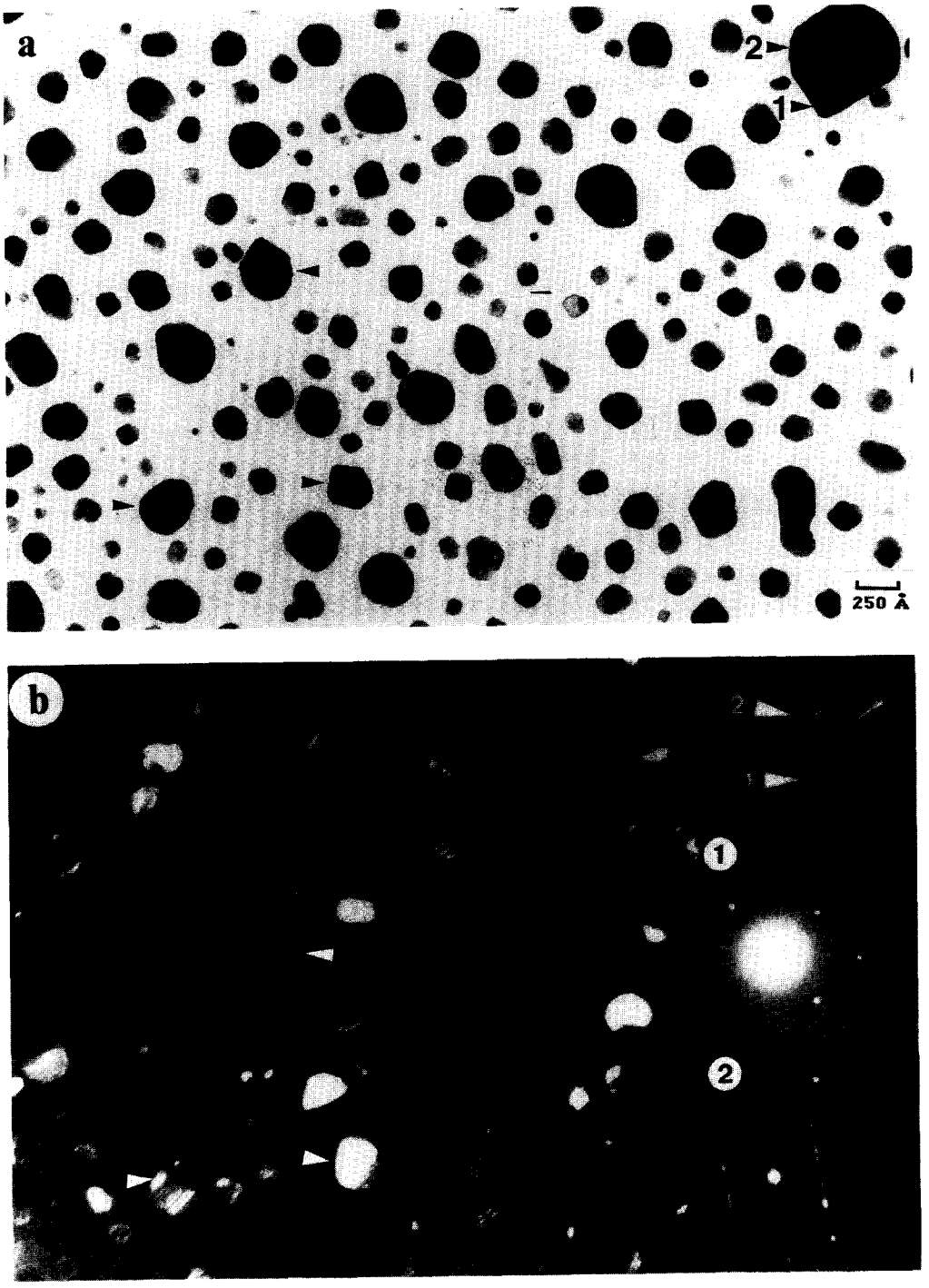

FIG. 1. (a) A typical transmission electron micrograph showing the segregated Pt 38 at.% Rh particles formed after treatment of an amorphous SiO_2 supported Pt–Rh film in H_2 at 650°C for 18 hr. Regions such as that marked "1" exhibit the characteristic cubic morphology of pure Pt while regions such as that marked "2" are highly defected and exhibit a nearly spherical shape. (b) The dark field image of (a) which shows the defected regions to be confined exclusively to the "spherical" parts of the particles. Inset 1, a microdiffraction pattern of a typical cubic region (marked 1) illustrates these regions to be fcc with a [100] zone axis. Inset 2, a microdiffraction pattern of a typical defected particle (region 2) shows the streaking indicative of staking faults.

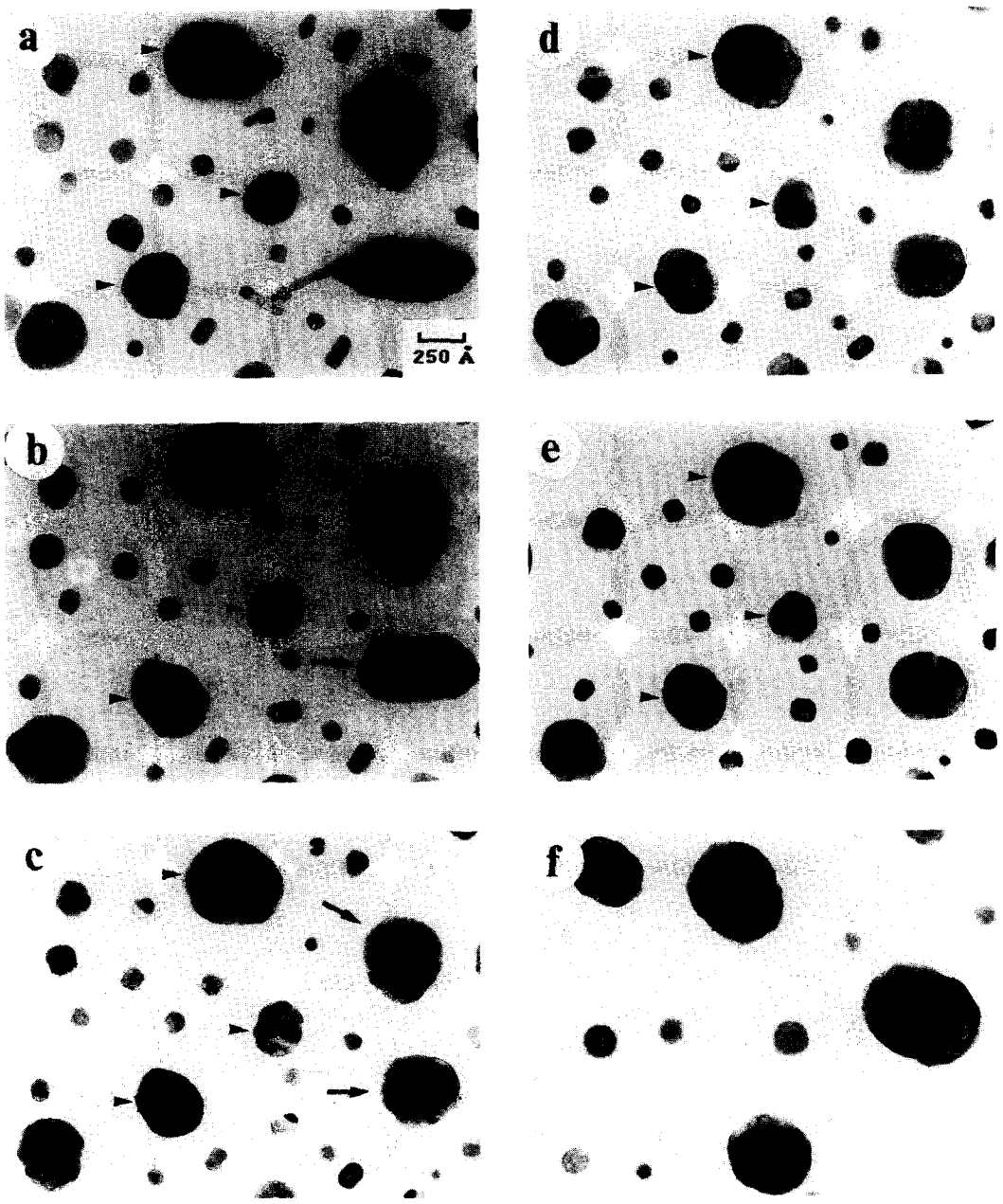

FIG. 2. Micrographs showing the microstructure evolution of a Pt 44 at.% Rh film on amorphous SiO_2 after treatment in H_2 at (a) 650°C, 4 hr; (b) 800°C, 1 hr; (c) 850°C, 5 hr; (d) 850°C, 22 hr; (e) 900°C, 5 hr; and (f) 1000°C, 17 hr. Most particles have two distinct regions, and several particles show three segregated regions, indicated by arrows.

Morphological Changes in Oxygen, Nitrogen, and Helium

Figure 3 shows the change in morphology of a 44 at.% Rh sample as a result of sequential treatments in H_2, O_2, and N_2. Figure 3a shows the characteristic segregation of particles after hydrogen treatment at 650°C for 12 hr. The electron diffraction

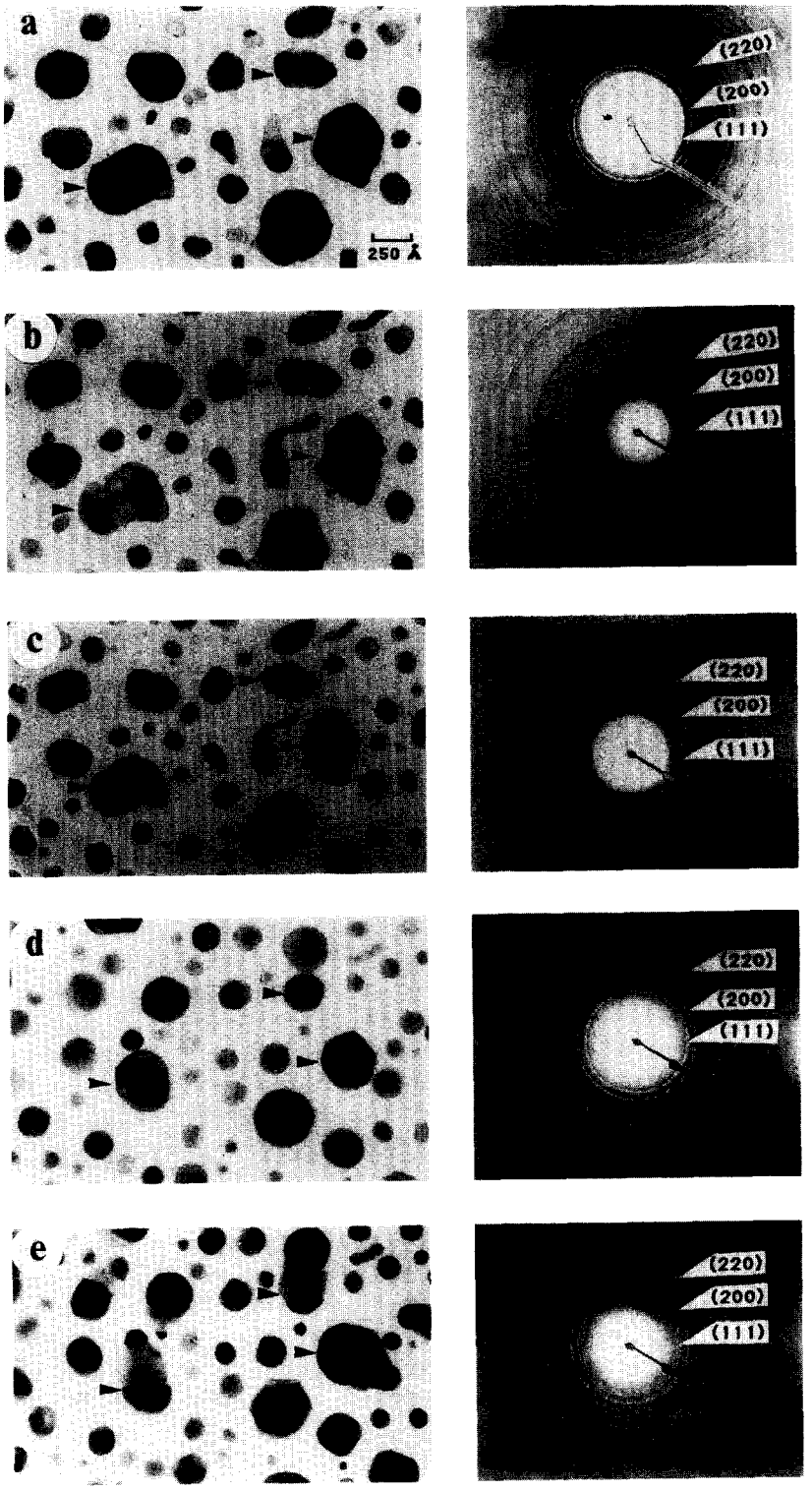

FIG. 3. Micrographs and accompanying diffraction patterns of a Pt 44 at.% Rh SiO_2 supported film after sequential treatments in (a) H_2 at 650°C for 12 hr, (b) O_2 at 300°C for 1 hr, (c) H_2 at 650°C for 18 hr, (d) N_2 at 650°C for 3 hr and (e) H_2 at 650°C for 18 hr. The (111), (200), and (220) diffraction rings of Pt are indicated where present in the diffraction patterns; (d) shows only the rings of an fcc alloy.

pattern (Fig. 3a) of this sample reveals rings which can be assigned to Pt metal (as shown) and also weaker, broad rings which are assigned to the defected region.

Mild treatment of the segregated particles in O_2 at 300°C for 1 hr (Fig. 3b) causes the breakup of the defected region, although the cubic regions remain unaltered and there is no detectable oxide formed. This change is accompanied by a significant change in the diffraction pattern which shows the disappearance of rings due to the defected alloy and the appearance of additional rings from an fcc alloy with a lattice parameter greater than that of Pt, but no rings assignable to an oxide. This alteration in the structure of the defected region is reversible. Subsequent heating in H_2 at 650°C for 18 hr returns the particles to the segregated form with some particles having very nearly the same structural configuration as before (Fig. 3c), although the Rh sections have changed considerably, in that the shape has changed and ring broadening is less apparent. This change in the Rh regions is indicated in the diffraction pattern by the appearance of several faint rings and the weakening of others associated with the alloy. The ability to reform the twinned region argues that it is an *equilibrium* structure in H_2 atmospheres.

Heating the two-phase alloy in N_2 at 650°C causes a dramatic change in the morphology of the particles as well as a significant change in the diffraction pattern. Figure 3d shows the sample of Fig. 3c, after it had gone through the $H_2 \rightarrow O_2 \rightarrow H_2 \rightarrow N_2$ sequence. After only 3 hr of heating, most of these same particles appear hexagonal or spherical in shape; none are segregated and only a few are twinned (Fig. 3d). The diffraction pattern is that of a single fcc alloy with a lattice constant of 3.87 Å (Fig. 3d). Treatment again with H_2 at 650°C results in the resegregation of the particles (Fig. 3e) and the reappearance of the complex diffraction pattern.

Figures 3d and 3e show the morphology change due to nitrogen treatment to be reversible as was the change due to oxygen treatment. In contrast, however, when a sample which had been treated in N_2 is then treated in O_2 at 300°C, little change in particle shapes is observed. This result is consistent with our previous work in which we reported the formation of a miscible Rh–Pt alloy upon treatment in N_2 which exhibited a morphology resistant to mild oxidation (*9*).

The dramatic difference between treatment in H_2 or N_2 suggests that one gas is "inert" while the other interacts in some way with the particles. To determine which interacted, we treated samples in He a totally inert atmosphere. Treatment in He results in the formation of morphological changes similar to those of treatment with N_2. Figures 4a and 4d show two Pt–Rh samples containing 39 at.% Rh after treatment in H_2 at 650°C for 17 hr. Figures 4b and 4e show the same samples after 2 hr at 650°C in helium and nitrogen, respectively. There is no significant difference in either sample or in their diffraction patterns (not shown). Subsequent treatment in hydrogen showed that both treatments result in reversible changes (Figs. 4c and 4f), indicating no significant difference between the helium and the nitrogen treatment.

Preparation from Salts

In all previous work, we have prepared metal and alloy particles from vacuum-evaporated films because this produces a highly uniform distribution of particles with accurately known loading. To test whether particle microstructure depended on the method of preparation, we also prepared Pt, Rh, and alloys from salts.

Figures 5a and 5b show pure Pt particles grown from metal and from $[Pt_3(CO)_6]_4^{2-}$, respectively, by heating in H_2 at 650°C for ~6 hr. In both cases all particles are cubes. The major difference is that the salt-prepared particles are not randomly distributed but form along lines in the SiO_2. This is evidently caused by the aggregation into small folds in the SiO_2 as the solution dries

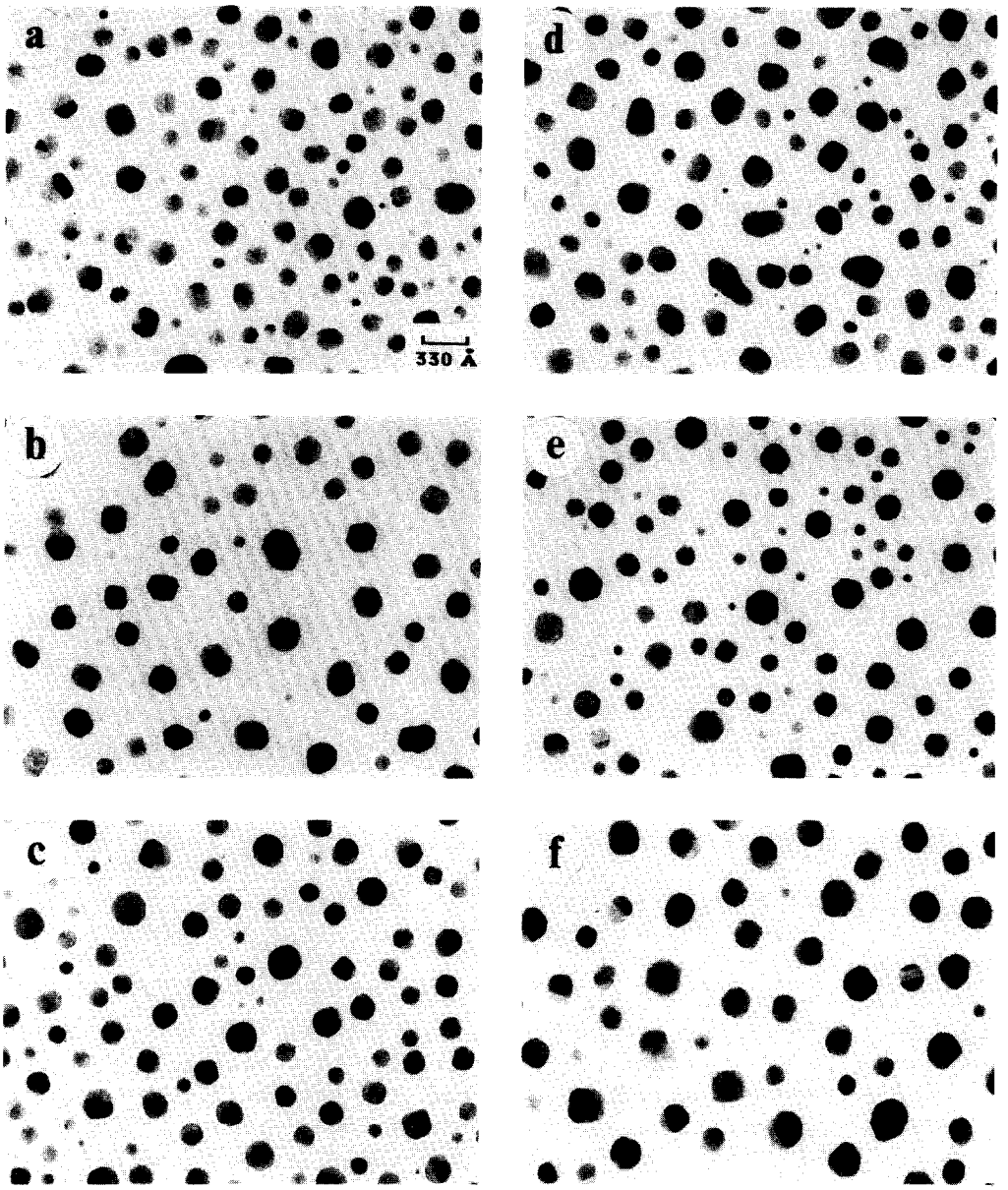

FIG. 4. Micrographs of two 39 at.% Rh SiO_2 films after sequential treatments at 650°C in (a) H_2, (b) He, and (c) H_2 for 17, 2, and 18 hr, respectively, and in (d) H_2, (e) N_2, and (f) H_2 for 17, 2, and 18 hr, respectively. No significant difference can be seen in the changes in particle structure for sequential heat treatments when He is substituted for N_2.

and the salt precipitates. In fact, these experiments demonstrate that particles as large as 1000 Å in diameter also form perfect cubes.

Figure 5c shows Rh particles prepared from $RhCl_3$. While particles vary more in size and density than in growth from metal films, they exhibit hexagonal shapes just as from metal deposition.

Figure 5d shows Pt–Rh particles prepared from $PtH_2Cl_6/RhCl_3$ solution. Sizes are highly nonuniform compared to deposi-

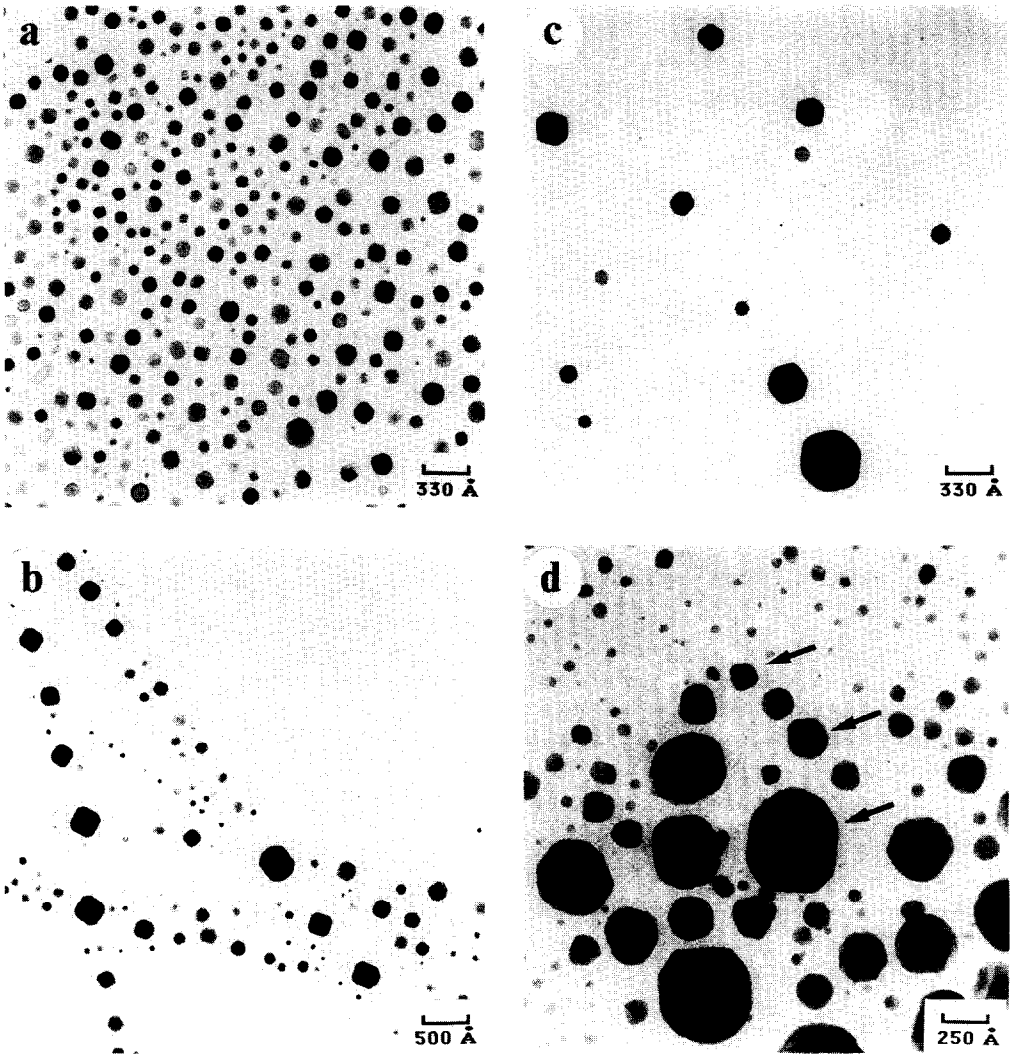

FIG. 5. Micrographs showing the characteristic morphologies of small particles of Pt, Rh, and the Pt–Rh alloy prepared from (a) Pt metal, (b) $[Pt_3(CO)_6]_4^{2-}$, (c) $RhCl_3$, and (d) $PtH_2Cl_6/RhCl_3$. Similar structures are observed for all preparation methods, and the alloy also exhibits cube and defected regions in each particle.

tion from the metals. In addition, some appear to be perfect cubes while others appear to be perfect hexagons which is suggestive of individual Pt particles and Rh particles. However, a number of particles exhibit the characteristic section of a cube and a sphere (see arrows). In some of these particles, the twin bands are also evident.

We conclude, therefore, that particle shapes and structures are essentially identical for preparation from evaporated metal films or from salts, at least after heating to ~600°C. However, metal films appear to give much more uniform particle sizes and distributions as well as more uniform alloy compositions.

DISCUSSION

Microstructure

It is evident that small particles of Pt–Rh supported on amorphous silica segregate into particles consisting of a cube-shaped Pt

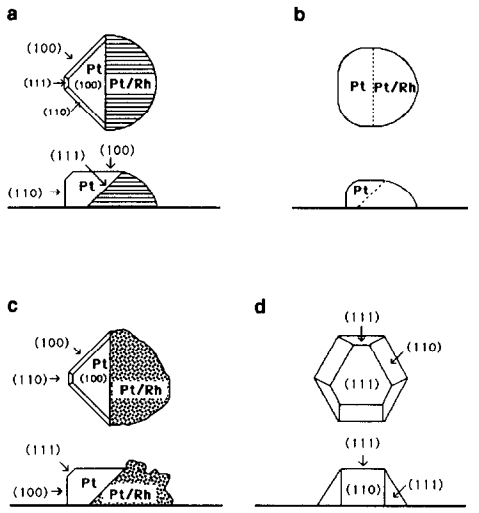

FIG. 6. Illustrations of the idealized morphologies of the Pt–Rh alloy on SiO_2, (a) the cube-shaped region of Pt and the defected alloy regions which form after sintering in H_2, (b) the loss of the characteristic shapes of each region following heat treatment in H_2 above 1000°C, (c) the breakup of the alloy structure and the unaltered Pt region following treatment in O_2 at 300°C, and (d) the hexagonal shape formed upon treatment in either N_2 or He at 650°C.

region and a highly twinned Pt–Rh alloy region when treated in a hydrogen atmosphere at a temperature of ~650°C and that this structure persists to ~1000°C. The relative size of each region appears to correlate with composition in that, as the amount of Rh increases, the relative size of the Pt region decreases. However, we did not attempt to determine a phase diagram by examining different compositions systematically.

The Pt region retains the characteristic cubic morphology of Pt particles grown in H_2 with (100) facets and [100] orientation with the silica (*7*), while the alloy region is highly defected and no specific orientation is apparent. This defected region exhibits in the bright field and dark field images the closely spaced lines characteristic of stacking faults (*17, 18*). The microdiffraction pattern for this region (inset 1, Fig. 1b) is a streaked pattern with hexagonal symmetry characteristic of the hcp structure found in stacking faults of fcc materials (*18, 19*). This information from microdiffraction and the ability to correlate the unstreaked rings of the alloy region with the rings of the pure Pt region of a given particle enable us to assign the streaked rings in the diffraction pattern of the Pt–Rh alloy.

The favored orientation of the interface between these two regions appears to be along the diagonal of the Pt cube, suggesting a (110) interface plane. However, close examination of many of these interfaces reveals that the interface is not a sharp line but instead there is a gradual loss in the intensity of the streaking as the Pt region is approached (Figs. 1a and 2b, regions 1 and 2, and Fig. 6a). This diminishing of intensity is consistent with the interface forming on the close-packed (111) planes, the energetically favored twinning planes of fcc materials (*19*), which are inclined to the electron beam. The interface may therefore be simply a (111) twin plane between the nearly perfect Pt cube and the highly twinned alloy.

Above 1000°C in H_2, the particles undergo a distinct change. The morphology of the Pt region is altered in shape and the defects of the alloy region coalesce to form single-phase particles which appear twinned and of roughly spherical shape. This transition is accompanied by the loss of many of the rings attributed to the defected alloy. We interpret this transformation to be the result of the formation of a more ordered alloy crystal (Fig. 6b) resulting from the reduction of stresses in the alloy itself (*19, 20*).

Mild oxygen treatment at 300°C results in the complete breakup of the alloy region while leaving the Pt region unaltered, as expected since Pt cannot be oxidized by heating in O_2 under these conditions (Fig. 6c). This breakup occurs under more mild conditions than we have observed previously for oxidation of Rh alone (*8*) and without evidence of the formation of a Rh_2O_3 phase in either the bright field image or the diffraction pattern. However, the oxide is al-

most certain to exist as a thin layer covering the alloy particles (*9, 21*). The presence of the defects in the alloy appears to facilitate the oxidation of the alloy under conditions too mild for the formation of substantial amounts of oxide from Rh alone. By comparison, samples which have been treated in N_2 prior to a similar O_2 treatment show no breakup of the particles at these temperatures.

Nitrogen treatment results in the formation of particles of roughly hexagonal shape and a diffraction pattern of a simple fcc alloy with a lattice constant between those of the Pt and Rh metals. Close examination of the bright field image (Fig. 3d) reveals that few of the particles exhibit any internal structure. It is evident that in N_2 the regions rapidly coalesce to form a solid solution of Pt and Rh (Fig. 6d) and prior treatment in H_2 does not alter this outcome.

Shapes of Pt Alloy Particles

Pure Rh particles exhibit nominally hexagonal shapes as expected for predominantly (111) planes while pure Pt particles exhibit cubic shapes because they form predominantly (100) planes. In the Pt–Rh alloy particles, the Pt region retains a cubic shape rather than reverting to a hexagonal or a spherical shape as one might expect for an fcc alloy. In this section we consider the implications of these shapes.

In small particles with fixed mass and phases, the equilibrium shape (*22–24*) is primarily determined by the facet morphology and can be expressed as

$$\Sigma\gamma_i A_i = \text{minimum},$$

where the summation over surface free energy γ_i is over all planes and interfaces of area A_i. Contributions from edges and corners should be significant only for particles less than ~20 Å in size (*25*).

For an isolated single-phase crystal or for a particle on a flat surface, the Wulff plot, which is a polar plot of γ versus crystallographic orientation, can be used to predict the shape of the particle (*23, 26*). The hexagonal shape of Rh and most fcc metals (Fig. 5c) confirms that it exhibits the geometry predicted; i.e., the low γ surfaces after treating in H_2 are the close-packed (111) surfaces. In contrast, the cube shape of Pt (Figs. 6a and 6b) shows that the (100) plane of Pt has the lowest γ in hydrogen as has been discussed elsewhere (*7, 8*).

For a particle on a planar support (*7*), the modified Wulff plot shows that specific planes at the interface should give a minimum particle-free energy, and this is also confirmed by formation of hexagonal outlines for most fcc metals including Rh for which the (111) plane is usually in contact with the support. However, for Pt the (100) plane and occasionally the (110) plane is in contact with either SiO_2 or Al_2O_3 supports, again because these planes give minimum free energy for the system (*7*).

For a multicomponent system the same arguments are valid except that γ_i is a function of composition. Adsorbates generally lower γ from the clean surface value. If the heat of adsorption is ΔH_i and its adsorption density is n_i, one should expect that

$$\gamma_i \cong \gamma_{0,i} - \Delta H_i n_i.$$

Since heats of adsorption and saturation densities are generally higher on open, high-index, high-γ planes, γ for these orientations should be *lowered most* by adsorption. Consequently the anisotropy in γ should generally be expected to *decrease* upon adsorption and the shape would therefore tend to change from a polyhedron to a sphere upon chemisorption. We used this argument previously to explain our observation that Pt particles transformed reversibly to spheres when heated in gases which would cause monolayer adsorption (*7*).

For a binary A–B alloy, a bond model of γ would predict

$$\gamma_i = \gamma_{iA}\theta_A + \gamma_{iB}(1 - \theta_A),$$

where γ_{iA} and γ_{iB} are surface free energies of pure A and B, respectively, and θ_A is the fraction of the surface layer covered by component A. These expressions ignore en-

tropy effects which should of course become important at higher temperatures.

For a Pt–Rh particle we expect that $\gamma_{Rh} > \gamma_{Pt}$ from published average values and from the fact that γ for metals should scale roughly with the melting temperature. Therefore a Pt–Rh alloy particle should be *surface enriched in Pt* compared to the bulk composition.

We do not know the bulk composition of the cube portion of these particles except that they certainly contain more Pt than the overall particles. Our observation of the exclusive formation of cubes strongly suggests that the (100) plane has the lowest γ and that the (100) plane forms the interface with SiO_2. We suggested previously that the (100) plane of Pt may have a lower γ than the (111) because it exhibits a hexagonal overlayer structure. Evidently, there is insufficient Rh in these alloy surfaces to increase γ of the (100) plane and thereby destabilize the cube shape of Pt.

Comparison of H_2, N_2, and He Treatments

Comparison of the results of N_2, H_2 and He treatments and the similarity of N_2 and He suggest that H_2 interacts with the alloy. One expects N_2 to exhibit inert behavior with respect to the alloy and its components because nitrogen has a low solubility and no nitrides are stable at these temperatures. However, the solubility of hydrogen in both Pt and Rh is also known to be very small (*27*), $\sim 4 \times 10^{-4}$ and $\sim 7 \times 10^{-4}$ at.%, respectively, at 650°C and hydrogen is not known to form hydrides with either metal.

However, H_2 is known to have a greater solubility in some alloys than their individual components (*28, 29*) including the Pd–Rh alloys (*30*). Hydrogen can cause lattice distortions in metals resulting in coherency stresses. When these stresses exceed a critical yield stress of the material, they result in the formation of dislocations (*20, 29*) and in some cases amorphization (*31*) and in others different crystal structures (*32, 33*).

It therefore appears likely that the anomalous behavior of H_2 is a result of an increased solubility of hydrogen in the alloy. The formation of structural defects in the alloy upon H_2 treatment appears to be a direct consequence of this increased solubility. The stresses from the hydrogen in the lattice and the differences in atomic size of the components (lattice constants for Pt and Rh are 3.923 and 3.803 Å, respectively (*34, 35*) may exceed the critical yield stress of the alloy, resulting in the formation of defects in the crystal. As the temperature is increased, hydrogen solubility decreases thereby decreasing stress and consequently the alloy exhibits a more defect free crystal as indicated by the changes seen in both the images and the diffraction pattern above 1000°C.

Phase Separation

The Pt and Rh have frequently been reported in the literature as being miscible in all proportions; however, it has been speculated from work with other platinum metals that a miscibility gap should exist at lower temperatures (<750°C) for the Pt–Rh alloys (*13, 14*). This miscibility gap is expected to be difficult to observe in macroscopic alloys since thermodynamic equilibrium is reached very slowly and X-ray diffraction can resolve phases only for crystals larger than 100 Å. However, it is expected that equilibrium can more readily be achieved in small particles because of the smaller distances atoms must diffuse.

We saw no evidence in this work or in our earlier work (*9*) of a miscibility gap when the alloy is treated in N_2 or He, but the presence of H_2 causes a segregation of the alloy particles into Pt regions and alloy regions. The presence of distinct Pt rings and alloy rings confirms that the segregation is still present up to 1000°C. This segregation indicates that H_2 induces a miscibility gap in the Pt–Rh system.

SUMMARY

These experiments show that Pt–Rh alloy particles formed from metal films or

salts produce segregated particles containing a characteristic cube-shaped Pt region and a highly defected spherical alloy region when treated in H_2. This segregation persists in H_2 up to ~1000°C. Mild treatment in O_2 at 300°C produces the breakup of the alloy region into smaller particles but leaves the cubic Pt region unaffected. Treatment in either N_2 or He at 650°C results in the reversible coalescence of the two regions to form single-phase particles with a roughly hexagonal to spherical shape. The cube-shaped morphology of Pt crystals in H_2 is independent of the method of deposition and is a stable geometry which persists upon alloying.

Morphologies are different in H_2 than in N_2 or He, and H_2 is shown to interact strongly with the alloy. We speculate that this behavior is a result of an increased hydrogen solubility in the alloy which induces a miscibility gap which causes segregation of the particles into Pt and alloy regions. However, we emphasize that we have no direct evidence that hydrogen dissolution in the particles causes the observed phase separation. The reported solubilities in both Pt and Rh are very small and the observed morphologies could also arise from an unknown species whose solubility in the alloy may be altered by the presence of H_2.

REFERENCES

1. Pullitzer, E. L., *Platinum Met. Rev.* **16,** 42 (1972).
2. Burch, R., *Platinum Met. Rev.* **22,** 57 (1978).
3. Sinfelt, J. H., U.S. 3,953,368.
4. Rasser, J. C. "Platinum–Iridium Reforming Catalysts." Delft Univ. Press, The Netherlands, 1977.
5. Taylor, K. C., and Schlatter, J. C., *J. Catal.* **63,** 53 (1980).
6. Schlatter, J. C., and Taylor, K. C., *J. Catal.* **49,** 42 (1977).
7. Wang, T., Lee, C., and Schmidt, L. D., Surf. Sci. **163,** 181 (1985).
8. Schmidt, L. D. and Lee, C. *in* "Catalyst Deactivation" (E. E. Petersen and A. T. Bell, Eds.), p. 297. Dekker, New York, 1987.
9. Chen, M., Wang, T., and Schmidt, L. D., *J. Catal.* **60,** 356 (1979).
10. Lee, C., Schmidt, L. D., Moulder, J. F., and Rusch, T. W., *J. Catal.* **99,** 472 (1986).
11. Lee, C., and Schmidt, L. D., *J. Catal.* **101,** 123 (1986).
12. Balseiro, C. A., and Moran-Lopez, J. L., *Surf. Sci.* **156,** 404 (1985).
13. Raub, E., *J. Less Comman Met.* **1,** 3 (1959).
14. "The Handbook of Binary Phase Diagrams," Vol. 4. General Electric Co., Gainesville, FL, 1/1980.
15. Guettler, R. D., Bellare, J. R., Davis, H. T., and Scriven, L. E., "Proceedings of the 45th Annual Meeting of the Electron Microscopy Society of America, 1987," San Francisco Press, Inc., San Francisco.
16. Beeston, B. E. P., Horne, R. W., and Markham, R., "Electron Diffraction and Optical Diffraction Techniques." North-Holland, Amsterdam, 1972.
17. Reimer, L., "Transmission Electron Microscopy." Springer-Verlag, New York/Berlin, 1984.
18. Hirsch, P., Howie, A., Nicholson, R. B., Pashley, D. W., and Whelan, M. J., "Electron Microscopy of Thin Crystals." Krieger, Melbourne, FL, 1977.
19. Hertzberg, R. W., "Deformation and Fracture Mechanics of Engineering Materials," 2nd ed. Wiley, New York, 1983.
20. Christian, J. W., "The Theory of Transformations in Metals and Alloys," 2nd ed. Pergamon, Elmsford, NY, 1975.
21. Wang, T., and Schmidt, L. D., *J. Catal.* **71,** 411 (1981).
22. Winterbottom, W. L., *Acta Metall.* **15,** 303 (1967).
23. Murr, L. E., "Interfacial Phenomena in Metals and Alloys." Addison–Wesley, Reading, MA, 1975.
24. Cahn, J. W., *Acta Metall.* **28,** 1333 (1980).
25. Marks, L. D., *Surf. Sci.* **150,** 358 (1985).
26. Herrington, C., *Phys. Rev.* **82,** 87 (1951).
27. *Bull. Alloy Phase Diagrams* **4,** 324 (1984).
28. Peisl, H., *in* "Hydrogen in Metals" (G. Alefeld, and J. Volkl, Eds.), Vol. I, p. 53. Springer-Verlag, New York/Berlin, 1978.
29. Lewis, F. A., *Platinum Met. Rev.* **26,** 121 (1982).
30. Grishina, T. M., *Zh. Fiz. Khim.* **57,** 1840 (1983).
31. Somenkov, V. A., and Irodova, A. V., *J. Less Comman Met.* **101,** 481 (1984).
32. Oestereicher, H., Clinton, J., and Bittner, H., *Mater. Res. Bull.* **11,** 1241 (1976).
33. Muller, H., Weymann, K., and Hartwig, P., *J. Less Comman Met.* **74,** 17 (1980).
34. ASTM, X-Ray Powder Data File, 4-802.
35. ASTM, X-Ray Powder Data File, 5-685.